Geoscientific
Instrumentation
Methods and
Data Systems
Discussions
Open Access

CONTINUOUS WAVELET TRANSFORM AND EULER DECONVOLUTION METHOD AND THEIR APPLICATION TO MAGNETIC FIELD DATA OF JHARIA COAL FIELD, INDIA

Arvind Singh and Upendra Kumar Singh

Department of Applied Geophysics, Indian School of Mines, Dhanbad, India-826004

1. Abstract

This paper deals the application of Continuous Wavelet Transform (CWT) and Euler deconvolution methods to estimate the source depth using magnetic anomalies. These methods are utilised mainly to focus on the fundamental issue for mapping the major coal seam and locating magnetic lineaments. These methods are tested and demonstrated on synthetic data and finally applied on field data from Jharia coal field. Prepared magnetic anomaly map that reflects clear tectonics control and nature of the underlying basement, demarcation of the basin, geological faults by steep gradients of magnetic anomaly. Analysis suggests that the CWT have a great utility in the magnetic data interpretation and the correlation between magnetic anomalies and geological features such as faults/joints and intrusive bodies over the basin. The CWT provides the consistent and reliable depth of the underlying basement with the results of Euler deconvolution and Tilt-depth methods without any priory information that is correlated well with borehole samples (Raja Rao, 1987).

One of the fundamental issues is to detect differences in susceptibility and density between rocks that contain ore deposits or hydrocarbons or coal. These differences are reflected in the gravity and magnetic anomalies and also delineation of structural features, which are interpreted using several techniques (Blakely and Simpson, 1986). One of the most important objective in the interpretation of potential field data is to improve the resolution of underlying source, delineating lateral change in magnetic susceptibilities that provides information not only on lithological changes but also on structural trends.

Summary of Comments on gi-201622_jharia_arvind-annoated.pdf

Page: 1

	Number: 1	Author: sanjay	Subject: Highlight	Date: 10/25/2016 11:04:07 AM

CWT technique can be use

	Number: 2	Author: sanjay	Subject: Sticky Note	Date: 10/23/2016 1:09:29 PM

what does mean by magnetic lineaments?
lineaments is a geological feature so magnetic lineaments is related to what?

	Number: 3	Author: sanjay	Subject: Highlight	Date: 10/23/2016 1:08:05 PM

	Number: 4	Author: sanjay	Subject: Sticky Note	Date: 10/23/2016 1:21:02 PM

pl explain that how basement structure or tectonic control can be find with intensity anomaly map.

	Number: 5	Author: sanjay	Subject: Highlight	Date: 10/23/2016 1:09:59 PM

Geoscientific
Instrumentation
Methods and
Data Systems

Open Access

Discussions

31   Especially, mapping the edges of causative bodies is fundamental to the application of

32   potential field data to geological mapping. The edge detection techniques are used to

33   distinguish between different sizes and different depths of the geological discontinuities

34   (Cooper and Cowan 2006, 2008; Perez et al. 2005; Ardestani 2010; Hsu et al. 1996, 2002;

35   Holschneider et al., 2003). The derivatives of magnetic data are used to enhance the edges

36   of anomalies and improve significantly the visibility of such features.

37   Sedimentary layer dominates the gravity and magnetic signature over Jharia Coal

38   field (Verma et al., 1973, 1976, 1979). Thus the difference between the depths estimated

39   using Euler deconvolution method (EDM) (Thompson 1982; Reid et al. 1990) and Tilt

40   Depth Method (TDM) technique (Salem et al., 2007; Cooper 2004, 2011) may help to

41   detect the thickness of the coalbed. Wavelet transform and Euler deconvolution method

42   has been theoretically demonstrated on magnetic data. These methods provide source

43   parameters such as the location, depth, geometry of geological bodies and interfaces in

44   an easy and effective way. However, it may be more difficult to characterize the source

45   properties in cases of extended sources (Sailhac et al., 2009).

46   These methods executed over Jharia coal field, Dhanbad, India. This area forms

47   an east west trending belt of Gondwana basin of Damodar valley at the north eastern part

48   of India. This study region is mostly coal rich area of Gondwana basin. Analysis on Jharia

49   coal field suggests that the magnetic anomalies provide encouraging results which are

50   well correlated with available gravity data and some borehole informations.

51

52   **2. Geology of Jharia coal field**

53   Geology of the Jharia coal basin is shown in Fig. 1. The basin has been formed

54   because of crustal subsidence during Gondwana periods (Fox, 1930). The coal field have

55   extension along the east west direction in Gondwana basin of Damodar valley at the north

56   eastern part of the India. Gondwana basin is surrounded by crystalline gneisses of several

57   categories from all the directions. Sedimentary strata have the inclination away from the

58   gneiss contact in this region. The sedimentary strata include the rocks which belong to

59   Talchir, Raniganj series, Barren-measures formation and Barakar series (Verma et al,

60   1979). Raniganj series, Barakar series and Talchir series including barren measures

61   formation covers area about 58 km^2, 218 km^2 and 181 km^2 respectively. Various

62   formations are shown in the Figure 1.

Number: 1   Author: sanjay   Subject: Highlight   Date: 10/24/2016 9:37:50 AM

Number: 2   Author: sanjay   Subject: Sticky Note   Date: 10/24/2016 9:38:13 AM
incomplete sentence.

63
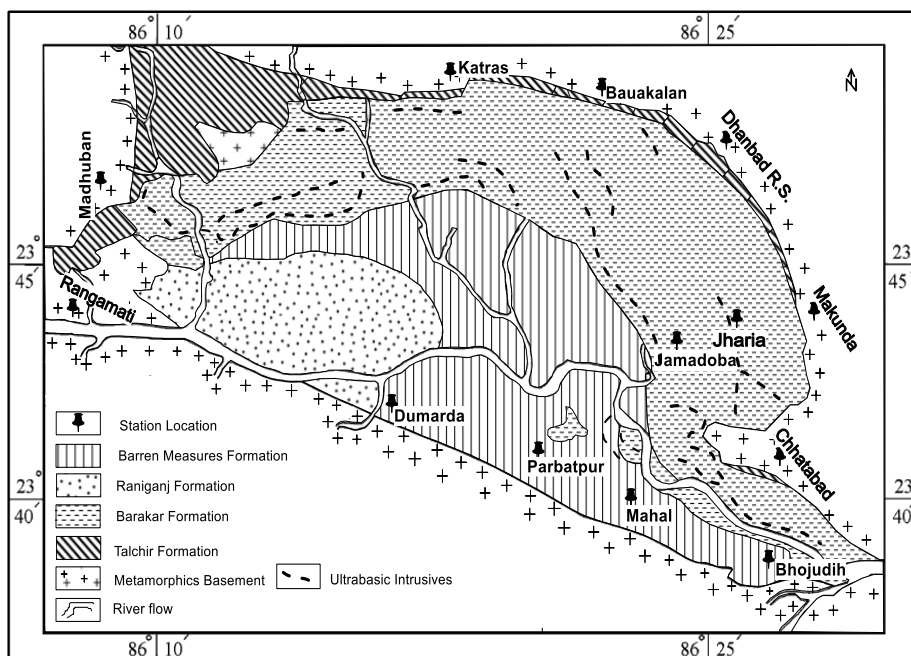
Figure 1: Geological map of Jharia coal field and surrounding regions, (after Verma et al, 1979)

64
65

66

67   Talchir and Barakar formation rest over northern margin and having dip towards
68   the southern margin. Barakar Series covers northern half of this coal field. Barakar series
69   produces the best quality coal in India. An elliptical outline is formed by Raniganj
70   formation in south western region of the coal field. Geology of the Jharia coal field has
71   been divided into many blocks like Parbatpur block, Mahuda block, Jarma and Monidih
72   block etc. There are many faults exist over Jharia coal field. A normal tensional fault
73   exists over the southern boundary. In the south western part of the basin Damodar river
74   (Fig. 1) flows very close to the southern boundary fault (Verma et al, 1973, 1979, Verma
75   and Ghosh, 1974).

76

Geoscientific
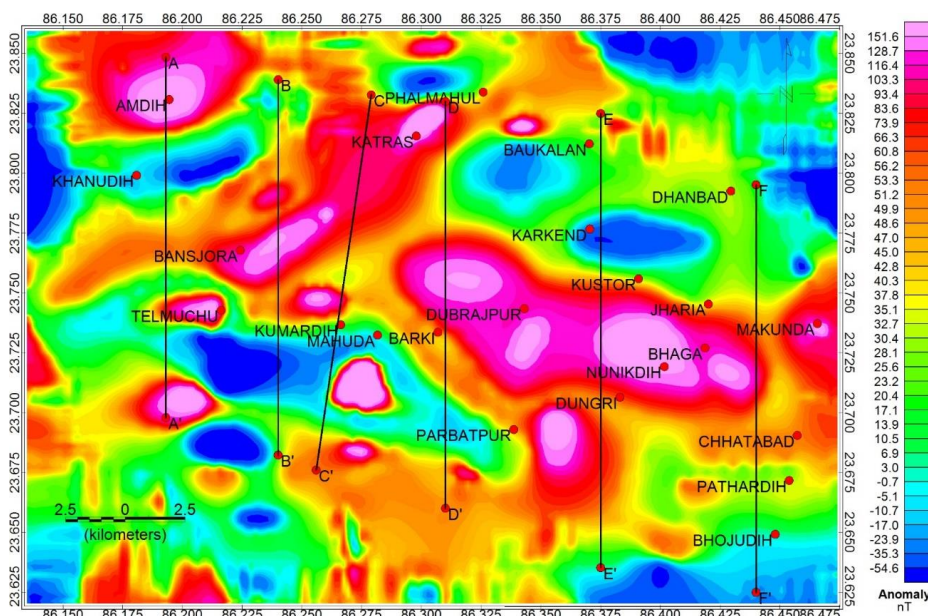Instrumentation
Methods and
Data Systems
Discussions
Open Access

Figure 2: Total magnetic field anomaly (nT) map and location of the profiles over Jharia
coal field and surrounding regions (after Verma et al., 1979).

The Magnetic data has been obtained from Verma et al (1979) to study the region. After, all necessary corrections, we prepared the total magnetic anomaly map with the help of magnetic data of this province as shown in Fig. 2. The map shows very sharp and irregular pattern outcrops, while over the basin the variations of magnetic anomalies are smooth and the northern part of the basin the magnetic anomalies over this region suggest that basin is identical to a curve. In the southern part, the anomalies are fairly parallel to the southern boundary fault and there is no clear indication of the trend of the anomalies in the south eastern part, which is probably due to its irregular faulting associated with Pathardih horst. Obviously the anomaly map reflects the sediments have been highly folded and faulted and coal seams have been highly deformed. A noticeable part of the magnetic anomaly is the presences of major anomalous source, which are ascribed to some features within the Precambrian basement underlying sediments.

🗨 Number: 1   Author: sanjay   Subject: Sticky Note   Date: 10/24/2016 10:06:52 AM

there are so many doubt about magnetic map.
is magnetic data is collected by author or used from verma et al 1979.
if verma et al then what correction has appiled in processed data.
what does mean by help of magnetic data?
what does mean by outcrops?
how directly magnetic map depicted about folding and faulting and most important about deformed?
the magnetic data can only depicts the high and low and gradient which can be due to heterogeneities present in the studies area.
rewrite the section.

T Number: 2   Author: sanjay   Subject: Highlight   Date: 10/24/2016 9:58:28 AM

---

96   **3. Methodologies**

97   **3(a). Continuous Wavelet Transform**

98   The continuous wavelet transform is the conversion of any signal into matrix

99   made of sum scaler products in Fourier space. Wavelet Transform method for potential

100   field has been established by Moreau et al. (1997, 1999). This method previously used

101   for homogeneous, isolated and extended potential field sources (Sailhac et al., 2009).

102   Chamoli (2006); Cooper (2006); Goyal and Tiwari (2014); Singh and Singh (2015) used

103   wavelet transform method on various synthetic as well as on field data. Method allows

104   Poisson group of wavelets as a mother wavelet in order to interpret the potential field

105   data. To analyse the signal by mother wavelet, a wavelet domain signal is decomposed

106   into the orthogonal wavelets of finite duration. The CWT coefficient W_t of a measured

107   potential $t(\text{x})$ is defined as the convolution product.

108   $$W[\psi,t](p,o) = \int_{R^n} \frac{1}{o^n} t(x)\psi\left[\frac{p-x}{o}\right]dx \qquad (1)$$

109   $$W[\psi,t](p,o) = (D_o\psi * t)(p) \qquad (2)$$

110   where ψ $(x \in R^n)$ is the wavelet to be analysed; x denotes the abscissa along the

111   particular profile line; $t(\text{x})$ indicates the potential field (gravity or magnetic anomaly);

112   $(o \in R^+)$ and p are the dilation and position parameter respectively. Dilation parameter

113   allows analysing wavelet to act as a band pass filter. Dilation operator D_o can be termed

114   as

115   $$D_o\psi(x) = \frac{1}{o^n}\psi\left(\frac{x}{o}\right) \qquad (3)$$

116   dilation D_o fulfils two properties given below

117   (i) $$W[\psi, D_\lambda t](p,o) = \frac{1}{\lambda^n} W[\psi,t]\left(\frac{p}{\lambda},\frac{o}{\lambda}\right) \qquad (4)$$

118   above equation states that the main mathematical asset of wavelet transform (i.e.
119   covariance of wavelet transforms with respect to the dilation) and
120
121   (ii)   Homogeneous function t of degree $\sigma \in R$ can be define as

122   $$t(\lambda,x) = \lambda^\sigma t(x) \forall \lambda > 0 \qquad (5)$$

123   after correlation equations (4) and (5) result homogeneous function (i.e. by recalling σ=-
124   n and σ=0, respectively)

125    $$(\lambda p, \lambda o)W[\psi, t] = \lambda^{\sigma} W[\psi, t](p, o)$$ (6)

126   Equation (6) represents that wavelet transform of a homogeneous function is
127   analogous to dilation and scale of any function $W(\psi, t)(p, o = consant)$ of the wavelet
128   transform. Moreau et al., (1999) suggest that the combinations of straight lines creates a
129   cone like outline at the location where $\left(\dfrac{\partial^m}{\partial p^m}\right)W(\psi, t)(p, o) = 0$ and apex of the outline is
130   the centre of homogeneity of the analysed function. The outlines in the Fig. (3) fulfils the
131   condition $\left(\dfrac{\partial^m}{\partial p^m}\right)W(\psi, t)(p, o) = 0$ are known as edges of wavelet transform or modulus
132   maxima lines.

133   Potential field signal analysed by CWT allows for estimation of depth and
134   homogeneous distribution order of the source generating the analysed signal. Source
135   depth is calculated through the intersection of the converging extrema lines (Fig. 3). In
136   addition to this, Moreau et al. (1997, 1999) established the Poisson semi group kernel
137    $K_o(x)$, which allows to carry on the harmonic field $t(x, z)$ from level z to the level z+o,
138   and expressed as upward continuation (Bhattacharyya, 1972).

139    $$P_o(x) = \frac{o}{\pi}\left(\frac{1}{o^2 + x^2}\right)$$ (7)

140   For wavelet analysis, let us consider a local homogeneous source $x = 0$ having depth
141    $z = z_{\alpha}$, of a potential field $t(x, z = 0)$. Moreau (1999) stated that the wavelet coefficients
142   of positions and dilations lie in the upper half plane follow a twice scaling rule with two
143   exponent parameters. Moreau (1997) explained the relationship between wavelet
144   coefficients at two altitudes and for any wavelets of homogeneous sources as

145    $$W[\psi, t](p, o) = \left(\frac{o}{o'}\right)^{\gamma}\left(\frac{o' + z_{\alpha}}{o + z_{\alpha}}\right)^{\beta} W\left(p\frac{o' + z_{\alpha}}{o + z_{\alpha}}, o'\right)$$ (8)

146   Where β= γ-σ-2 indicates the holder exponent, o and o′ denote different altitudes
147   while Z_{α} signifies the depth of the causative source. Equations (6) and (8) have additional
148   value in dilation and scaling in right hand side causes geometrical conversion of equation

149   (8). Due to geometrical conversion the cone like outline joins at source depth because of

150   the negative dilation o=z_α. Therefore, Poisson group of wavelets used on potential field

151   demonstrate modest assets and can be applied to find the causative source without any

152   prior information. CWT gives an idea to describe edges of the extended body. Also, it

153   offers quick and consistent results about extended and isolated source depth with location.

154   Wavelet analysis plays key role in depth estimation of potential field. When order of γ

155   increases then obtained source depth appears shallower. For $\gamma=1$, outlines of the cone

156   have the point of intersection at barycentre of the prismatic source. CWT can resolve the

157   noisy and non-stationary dataset very well (Moreau; 1997, 1999) and magnetic data can

158   also be analysed without any reduction to pole.

159

160   **3(b). Euler deconvolution Method**

161   Euler deconvolution was first developed for interpretation of magnetic profile data

162   by Thompson (1982) and later Reid et al. (1990) extended its approach to gridded

163   magnetic data. Reid et al. (1990) developed the special case for magnetic field of a contact

164   of finite depth extent and coined the term "Euler deconvolution". Klingele et al. (1991)

165   and Zhang et al. (2000) used it over gravity vertical gradient and tenser gravity gradient

166   respectively. Moreover, it has been generalised by Mushayandebvu et al. (2001, 2004)

167   and Rawat (1996) executed further to investigate the wider range of source nature. Since

168   then, it has been adapted and improved to interpret the gravity data by Keating (1998).

169   Euler Deconvolution Method (EDM) makes rapid depth estimations from magnetic and

170   gravity data in grid form using Euler´s homogeneity relation (Thompson, 1982; Reid et

171   al., 1990; Barbosa et al., 1999). Euler deconvolution is insensitive to magnetic inclination,

172   declination and remanent magnetisation and is very suitable for 3D analyses (Keating,

173   1998; Mushayandebvu et al., 2004; Stavrev and Reid, 2007; Melo et al., 2013, Silva, et

174   al., 2001).

175

176   The global acceptance of Euler deconvolution is mainly due to its simplicity of

177   implementation and use, making it the tool of choice for a quick and reliable tool of

178   interpretation for potential field data (FitzGerald et al., 2004; Gerovska and Arauzo

179   Bravo, 2003) and to find the source information in terms of depth and geological

180   structure. Euler deconvolution uses three orthogonal gradients of any potential quantity

181   as well as the potential quantity itself to determine depths and locations of a source body.

182   This method primarily responds to the gradients in the data and effectively traces the edge

183   and defines the depth of the source body. Reid et al., (1990) and Thompson (1982) defined

184   the 3-D Euler equation as.

185

186   $$(x - x_0)\frac{dF}{dx} + (y - y_0)\frac{dF}{dy} + (z - z_0)\frac{dF}{dz} + NF = 0 \qquad (9)$$

187   Where (x_0, y_0, z_0) is the location of magnetic source whose total magnetic field

188   (F) is observed at (x, y, z). The values $\frac{dF}{dx}$, $\frac{dF}{dy}$ and $\frac{dF}{dz}$ are the measured

189   magnetic gradients along the x, y, and z directions. Euler deconvolution adds an extra

190   dimension to the interpretation. It estimates a set of (x, y, z) points that, ideally, fall inside

191   the source of the anomaly. Euler deconvolution requires the x, y, and z derivatives of the

192   data and a parameter called the structural index (SI) N (N is non-negative integer). SI

193   defines the anomaly attenuation rate at the observation point and depends on the geometry

194   of the source. The SI is an integer number that is related to the homogeneity of the

195   potential field and varies for different fields and source types (Stavrev and Reid, 2007;

196   Barbosa et al., 1999 and Melo et al., 2013). For example, in the case of total field magnetic

197   anomaly data, a dike is represented by an SI of 1, whereas a sphere is represented by an

198   SI of 3.

199   The source points that are calculated as solutions by EDM are positioned at the

200   estimated edge of the susceptibility inhomogeneities. Thus, the EDM relies on the

201   derivatives of the magnetic data, the resulting depth estimates relate mainly to the areas

202   of basement heterogeneities identified as distinct sources of the field. The first vertical

203   gradient of magnetic data is calculated by using the fast Fourier transform (FFT) method

204   (Gunn, 1975). The vertical and horizontal derivatives of the first vertical gradient,

205   essential for the calculation of Eq. (9), are also been calculated using the FFT method.

206   The horizontal source locations from EDM solutions can be used for explanation of

207   lithological and structural trends. A location in the map where these solutions tend to

208   make cluster is considered to be the most probable location of the source.

209   Equation (9) can be explained in terms of least square to estimate the source

210   coordinates and structure. Since the absolute value anomalous field (F) is barely identified

Geoscientific
Instrumentation
Methods and
Data Systems
Discussions

Open Access

211   so equation (9) cannot be used directly over the observed data. Moreover, according to

212   Thompson, (1982) equation (9) does not explain the regional or background magnetic

213   field due to adjacent source, so obtained solutions may be unreliable and may vary from

214   their accurate location.

215   For 2-D model, estimation of total magnetic field (F) and its derivatives at all

216   points of data value provide the linear equation with unknown coordinates (x_0, z_0), where

217   x_0, z_0 represents location and depth of the magnetic source respectively.

218   Using Taylor series unidentified regional field (E) can be described as follows

219   $$E(x, y) = E_0 + x\frac{\partial E}{\partial x} + y\frac{\partial E}{\partial y} + K(2) \tag{10}$$

220   Where E_0 and $K(2)$ represent the constant background for definite window and

221   other higher order values in Taylor series expansion. The resultant anomalous field (F)

222   can now be specified as the difference between the observed magnetic field (O) and

223   regional magnetic field (E).

224   $$F = O - E \tag{11}$$

225   Now after revision modified Euler equation can be specified as

226   $$O \equiv (x - x_0)\frac{d(O - E)}{dx} + (y - y_0)\frac{d(O - E)}{dy} + (z - z_0)\frac{d(O - E)}{dz} + N(O - E) = 0 \tag{12}$$

227   According to Thompson (1982), Silva et al. (2003) and Reid et al. (1990), Euler

228   equation provides satisfactory results by considering the first order term in Taylor series

229   expansion. Also, Euler equation converts nonlinear and is resolved linearly by supposing

230   tentative values of the structural index (Stavrev, 1997). Higher order term of Taylor series

231   expansion provides the solution when singular points are closely spaced to each other

232   (e.g. in the case of the multiple fracture, sill etc.). In this case postulation of linear

233   background discontinues and needs higher order terms of Taylor series expansion for

234   reasonable result.

235   Dewangan et al. (2007); Gerovska, and Arauzo Bravo (2003) chose the second

236   order terms of the Taylor series expansion and favour to procedure of rational calculation

237   in which the infinite Taylor series expansion is estimated by two polynomials (one lies in

238   numerator and other one in denominator). Kopal (1961) suggested that the maximum

239   accuracy in rational calculation may be possible when the polynomials of numerator and

Geoscientific
Instrumentation
Methods and
Data Systems

Discussions

Open Access

240   denominator holds the same power. The rational function is used to calculate the

241   background, this function can be defined as

242
$$E(x, y) = \left(\frac{E_0 + ax + by}{1 + cy + dy} \right) \qquad\qquad (13)$$

243   Where, a, b, c, d and E_0 are the unknown parameter. Comparison of the value of

244   equation (13) and equation (12) generates another nonlinear Euler equation which

245   provides the source depth, location and structural index (Coleman and Li, 1996, Williams

246   et al., 2003). All the variation on Euler deconvolution includes working through profile

247   as well as gridded data set using moving window (each window position is a set of linear

248   equation which generates the solution to locate the source in plan and depth). The

249   advantage of this method is that source magnetization direction and its result are not

250   affected by the presence of remanence (Ravat, 1996). Moreover, it can be further used as

251   inversion algorithm and the design rules based on mathematical analysis are proposed by

252   Reid et al. (2014) must be considered to analyse the potential field (gravity and

253   magnetics).

254

255   **4. Modelling and Inversion of Gravity and Magnetic data**

256   It is difficult to separate two anomaly sources with conventional method when the

257   spatial scales of the sources are similar. Therefore, in order to ~~explore new sources,~~[1] it is

258   necessary to study the ~~inversion~~[2] method and technique of two layer interfaces for potential

259   fields (gravity and magnetic). ~~If the basement consists of both a density and a magnetic~~

260   ~~interface, significant tectonic information about the source depth can be revealed through~~

261   ~~joint gravity and magnetic inversion by including the information of magnetic basement,~~

262   ~~minimizing the inversion ambiguity, and enhancing the inversion reliability.~~[3]

263   Joint gravity and magnetic inversion methods started by Bott and Ingles (1972)

264   by using an equivalent layer approach to find the variation in magnetization and density

265   ratio of sources at the latter stage of the last century. Moreover, Menichetti and Guillen

266   (1983) used a generalized inversion method to define sources shape for the 2.5D case.

267   Zeyen and Pous (1993) deliberate the joint inversion problem on the basis of a priori

268   information such as density, susceptibility and remnant magnetization of buried source.

269   Zhang et al. (1993) established a method to invert gravity and magnetic data of the same

Number: 1	Author: sanjay	Subject: Replacement Text	Date: 10/24/2016 1:34:59 PM

what new source?

Number: 2	Author: sanjay	Subject: Replacement Text	Date: 10/24/2016 1:34:42 PM

inversion is not a method.

Number: 3	Author: sanjay	Subject: Replacement Text	Date: 10/24/2016 1:46:51 PM

Not clear.

Geoscientific
Instrumentation
Methods and
Data Systems
Discussions
Open Access

270   layer with density and magnetism and developed a general linear integral inversion

271   method. Gallardo Delgado et al. (2003) extended the 3D approach to include a density

272   variation with depth and the magnetization direction as unknown parameters. In order to

273   determine the topography of an interface of constant density and magnetization contrast

274   a damped least squares method was used by Pilkington (2006) for joint inversion of

275   gravity and magnetic data.

276   Wu et al. (2007) proposed the concept of a joint gravity and magnetic inversion

277   of a variable density interface which better matches with actual geologic conditions.

278   Practically, it is difficult to describe the nature of the misfit function or cost function as it

279   relates to the results and appraisal of geophysical inverse problem. Fernandez Martinez

280   et al., (2012, 2013) described the uncertainty in linear and nonlinear least squares inverse

281   problems and proposed new insights to understand uncertainty in inverse problem very

282   effectively. Jiang Fan et al. (2008) proposed and explain the effectiveness of the method

283   of joint gravity and magnetic inversion for two layer models by associating the thickness

284   changes and position of the middle layer and anomaly.

285

286   **5. Application of CWT to Synthetic Magnetic Anomaly**

287   The synthetic examples demonstrate the application of the CWT technique on the

288   magnetic anomaly due to isolated and extended homogeneous magnetic sources at the

289   position at 300 m having depth about 20 m. First analysis (shown in Fig. 3) corresponds

290   to the magnetic anomaly of a finite length vertical dipole. The wavelet coefficients of

291   magnetic field due to vertical dipole computed with the help of wavelet is shown in this

292   figure (for horizontal derivative $\gamma=1$) which shows a cone like structure. Wavelet

293   transform of the potential field due to homogeneous source follows a geometrical

294   property which allows an easy estimation of source depth and location. The examples

295   demonstrated could correspond to the zero remanent magnetization with all

296   magnetization being induced. To understand the behaviour of the modulus maxima of

297   CWT over of the magnetic anomaly due to the anomalous sources, the CWT is presented

298   for various field examples. The converging point of ridges gives depth and location of the
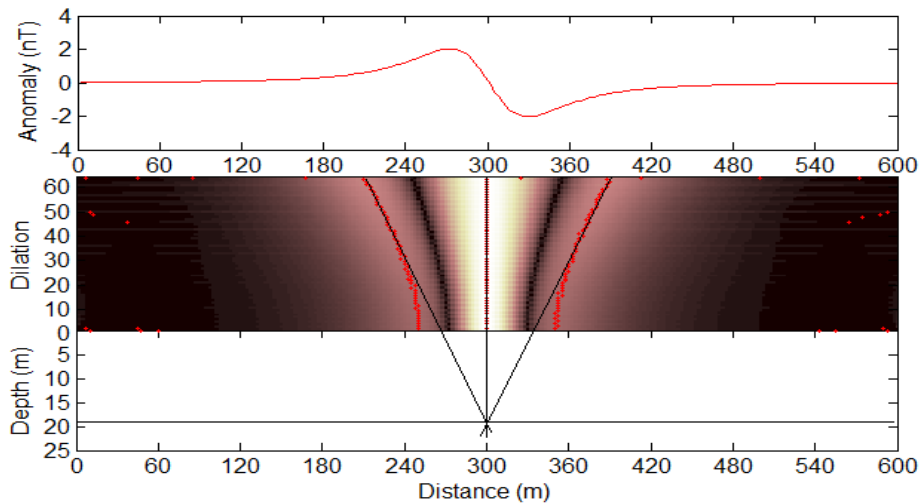
299   vertical dipole.

300

301

302   Figure 3: Synthetic magnetic anomaly of isolated extended source and depth estimation
303   by Wavelet transform for a Poisson wavelet for γ=1 with mathematical
304   expression k(x) =-[x (2/π)]/ (1+x^2)^2.

305

306   The wavelet coefficients are computed by applying CWT to the anomaly. Fig. 4
307   shows the calculated values of CWT coefficients for different dilations (1-64.5) of
308   magnetic anomaly. The maxima of modulus of CWT provide cone like structures and are
309   clearly shown which points towards the position of the upper corner of the model. On the
310   other hand, whereas an approximate horizontal location has been estimated, an
311   intersection of modulus maxima lines in the subsurface has placed below the base line
312   (a=0) to mark the depth of the source, where a is dilation.

313   Also, example illustrates the application of wavelet transform to potential fields
314   (horizontal derivative, γ=1) makes a cone like shape and ridges of the cone join below the
315   base line or to homogeneity centre of the source, where y-scale represents the dilation.
316   The point where ridges joins mark the depth and location and of the vertical dipole. It is
317   detected that homogeneous source retains a geometrical possession after execution of
318   wavelet transform on potential field. This makes a straightforward interpretation about
319   depth and location of causative body. In order to perform wavelet analysis on field data,
320   it has been tested on noisy data with 1%, 2%, 5%, 10% noise in the potential source data

321   obtained because of vertical dipole [Fig. 4 (a), (b), (c), (d)]. It is clear that Wavelet

322   analysis provides the exact depth and location of the source.

323
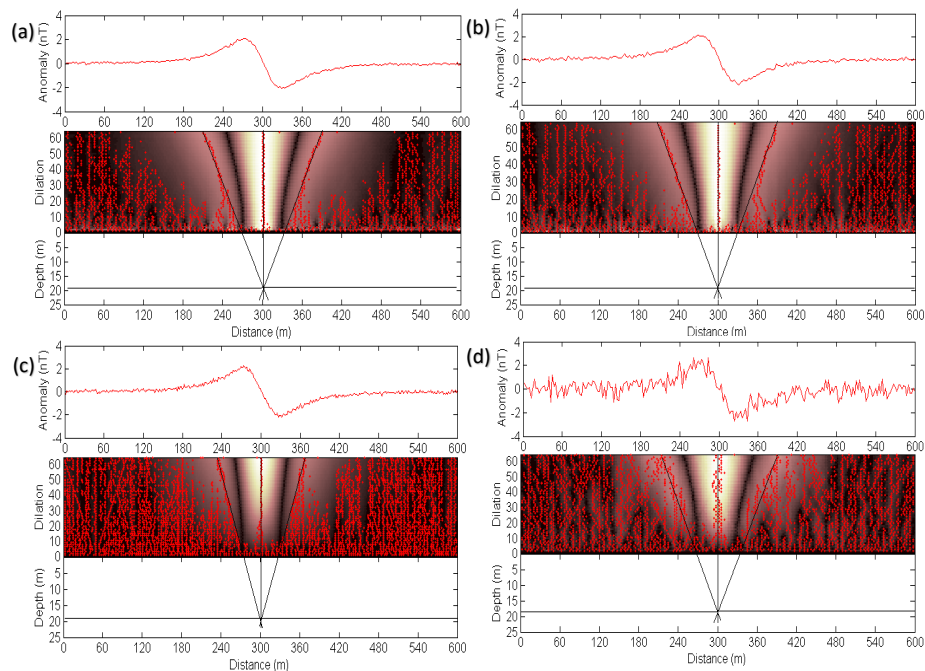
324

325   Figure 4: (a) magnetic anomaly with 1% noise (b) magnetic anomaly with 2% noise (c)

326   magnetic anomaly with 5% noise (d) magnetic anomaly with 10% noise.

327

6. Application of CWT to magnetic field anomaly from Jharia coal field

329   The CWT and EDM are applied on field magnetic anomaly collected from Jharia

330   Coal Field and surrounding regions, Dhanbad, India. For CWT analysis six profiles (AA',

331   BB', CC', DD', EE' and FF') have been selected, which cover the entire coal field. Fig. 2

332   shows the magnetic anomaly map, in which a number of anomalous sources such as

333   extension, direction of the bodies, geological faults/fold and tectonic signature has been

334   shown. These anomalies can be adequately explained by assuming an underlying body

335   having susceptibility contrast with respect to its surroundings and which is polarized in

336   N-S direction. The positive anomaly in the northern part of the basin is clearly seen in the

337   profile.

Number: 1   Author: sanjay   Subject: Sticky Note   Date: 10/24/2016 10:38:23 AM

if noise level is more then 10% then still will we get the same convergence depth?
if not then what maximum level accepted/resolve by present technique?

Number: 2   Author: sanjay   Subject: Highlight   Date: 10/24/2016 10:39:06 AM

Number: 3   Author: sanjay   Subject: Sticky Note   Date: 10/24/2016 10:43:53 AM

remove the sentence.
anomaly map only depicts high and low which might be possible relation with know surfacial geological structure and extended upto certain depth.
magnetic anomaly map can not directly indication of tectonic signature.

Geoscientific
Instrumentation
Methods and
Data Systems
Discussions
Open Access

338   The Remanence or remanent magnetization or residual magnetism of the body also [1]

339   appears to contribute to the anomaly. It is interesting to note that in the region [2] of this

340   magnetic anomaly a number of dykes and sills are found to be intrusive into the sediments [3]

341   as shown in Fig 2. This anomaly therefore could be ascribed to the presence of a basic or [4]

342   ultrabasic body which could be source for the basic dykes and sills which intruded into

343   the basin during Gondwana times. Alternatively, this anomaly could also represent a basic

344   intrusive of Precambrian age underlying the sediments. There are practically no basic

345   intrusive present in the region of positive anomaly. Therefore, this anomaly could be more

346   definitely ascribed to an intrusive body of Precambrian age Verma et al. (1979). [5]

347

348   **7. Results and discussion**

349   In order to check the reliability of the interpreted results obtained from Euler

350   deconvolution, CWT and geological sections construction information collected from

351   published results of boreholes drilled by Geological Society of India (G.S.I.), Bharat

352   Coking Coal Limited (B.C.C.L.), National Coal Development Corporation (N.C.D.C.),

353   Central Mines Planning and Design Institute (C.M.P.D.I). Therefore, the depth to the

354   basement configuration inferred from gravity data as well as drilled borehole information

355   discussed below.

356   Jharia coalfield and surrounding areas have been considered to estimate the source

357   depths on the basis of technique of intersections of modulus maxima lines of CWT. The

358   mean depths of causative sources along the profile AA′ (passes east of the Khanudih and

359   west of the Telmuchu and Bansjora region through Amdih over western most part of the

360   Jharia coal field, shown in Fig. 2) calculated from the CWT [Fig. 5 (i) (a)] and Daubechies

361   wavelet method [Fig. 5 (i) (b)] varies from 0.2 km to 0.45 km. Profile AA′ shows that

362   there is fault near the north-western part of the basin.

363   Magnetic Field Inclination, Declination and Azimuth Angle (clockwise from True

364   North) of this profile are 36.44°, -0.11° and 268.48° respectively. Anomaly hike a [6] out 77

365   nT between borehole JM-4 and JK-26 has been observed because of a number of basic

366   intrusive bodies belong to Satpura cycle exist over the area. Jharia coalfield consist of

367   peridotites in the forms of sills as well as dykes. Dolerite dykes are very common in

368   western part of this coalfield.

Number: 1   Author: sanjay   Subject: Sticky Note   Date: 10/24/2016 12:33:20 PM

remanance magnetization only effect the direction of magnetization and its gradient field.
what is mean by residual magnetism and how its contibute the total magnetic field.
provide the references.

Number: 2   Author: sanjay   Subject: Cross-Out Date: 10/24/2016 12:33:22 PM

Number: 3   Author: sanjay   Subject: Inserted Text   Date: 10/24/2016 12:33:29 PM

Number: 4   Author: sanjay   Subject: Replacement Text   Date: 10/24/2016 12:35:20 PM

what does meant by intrusive into sediments.
rewrite the sentence.

Number: 5   Author: sanjay   Subject: Replacement Text   Date: 10/24/2016 12:37:16 PM

it does not make any sense to discuss beyond the scope of present article.

Number: 6   Author: sanjay   Subject: Replacement Text   Date: 10/24/2016 2:28:40 PM

what does mean by hike?

369   Central part shows flat sedimentary region and magnetic anomaly shows high

370   value on either side of the profile. Raniganj formation exists on southern side whereas

371   Talchir formation exists on the northern side of this profile. However, the Barren-

372   Measures and the Barakar formations are lies in between the Raniganj and the Talchir

373   formations. There is an intrusion of Archean metamorphics in Talchir formation which

374   shows as outcrop over the surface near Amdih [Fig 5 (ii)]. The some of the bore holes

375   provide the information about the metamorphics along this profile. The maximum

376   thickness of the sediment along this profile is observed about 0.8 km.

377   Bore holes JM-1, JM-4 and JK-26 are located close to this profile, which touches

378   metamorphics at the depth about 0.4 km 0.55 km and 0.3 km respectively. These bore 1

379   hole are located west of Bansjora and Telmuchu. The depth to the basement obtained

380   from magnetic data is nearly equal to the depth obtained from gravity data along these

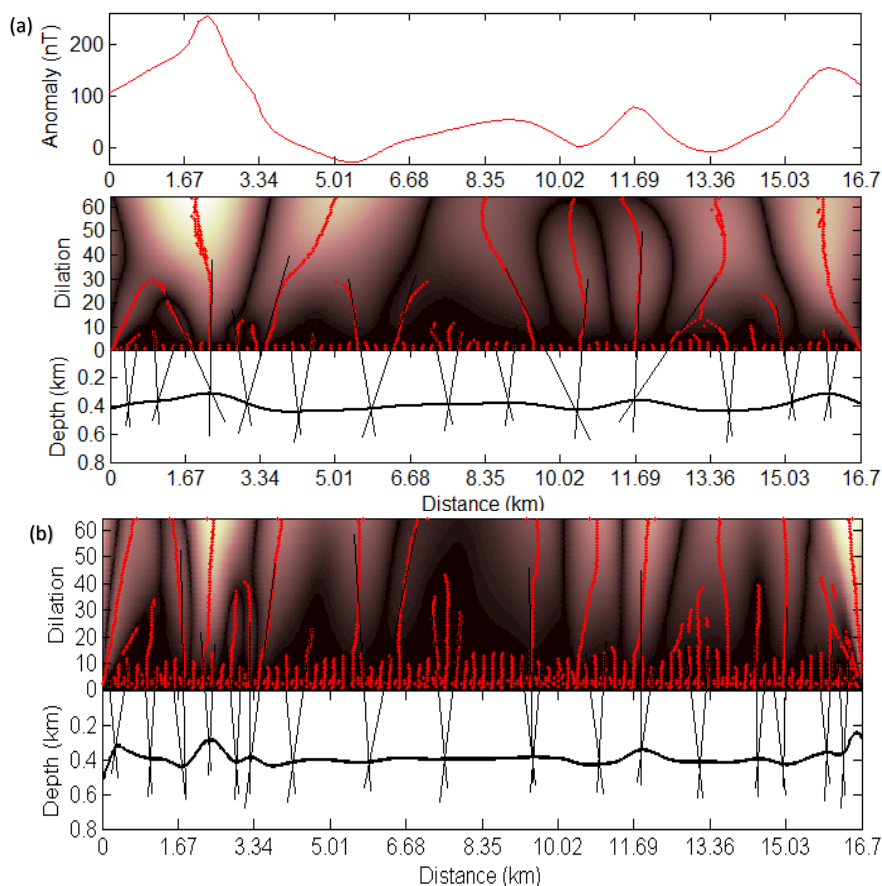381   profiles (Singh and Singh, 2015).

382

Number: 1　　　　Author: sanjay　　　　Subject: Replacement Text　　　Date: 10/24/2016 2:29:55 PM
bore-

383
384

385   Figure 5 (i): (a) Magnetic anomaly across the profile AA′ (drawn in Fig. 2) and depth

386   estimation by Continuous Wavelet Transform, (b) Depth estimation by

387   Daubechies wavelet.

388

389
390
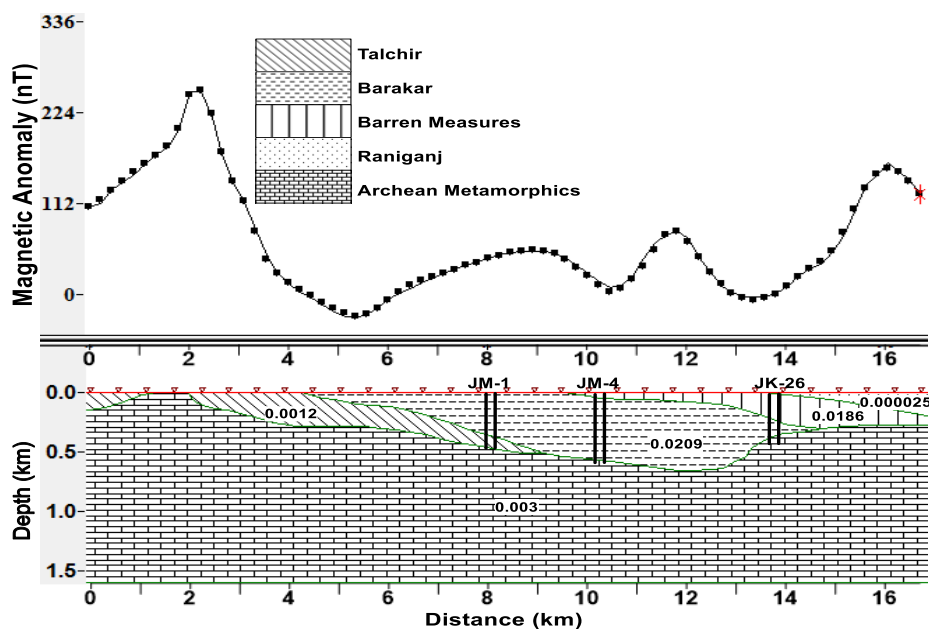391   Figure 5 (ii): 2D-model of the Profile AA′ drawn in Fig. 2.

392

393   The mean depths of causative sources along the profile BB′ (passes east of

394   Telmuchu and Bansjora and west of Kumardih region, shown in Fig. 2) calculated from

395   the CWT [Fig. 6 (i) (a)] and Daubechies wavelet [Fig. 6 (i) (b)] varies from 1.3 km to 2.5

396   km. Central part of the basin shows the abrupt changes in the magnetic anomaly.

397

398   Profile BB′ illustrates about the Barakar, the Raniganj, the Talchir and the Barren-

399   Measures. The barren measures is found in between the Barakar and Raniganj formation

400   which shows the outcrops in both sides of the Raniganj formation. Also, there is an

401   intrusion of Talchir formation has been found in Archean metamorphics and Barakar

402   formation at northern end of the profile [Fig. 6 (ii)]. There is a sloppy nature exist on both

403   side of the profile. The major portion of this area is dominated by the Raniganj and the

404   Barakar formations. The estimated thickness of the sediments is about 2.3 km over the

405   Raniganj formation.

406   Magnetic Field Inclination, Declination and Azimuth Angle of this profile are

407   36.42º, -0.11º and 268.5º respectively. This profile passes through two faults between

408   metamorphics and sediment. One is at southern end while another one at northern end of

409   the profile. Faults are indicated by steep gradient of magnetic anomaly. There are

410   Gondwana basin trapes are normally magnetized. Raniganj formation infested with

411   numerous dykes and sills. Magnetic anomaly hike about 103 nT and 162 nT south east

412   and east of Bansjora represent the occurrence of Precambrian basement underlying he

413   sediments.

414   logical section along this profile BB′ is deduced from analysis of gravity data,

415   available geological information and bore hole information. The bore hole JK-7 and JM-

416   8 are located near this profile. From the bore hole JM-7, it is obtained that maximum

417   thickness of the Raniganj formation is about 0.220 km and Barren-Measures lies below

418   it. It touches the Barakar formation at the depth about 1.2 km near east of Bansjora.

419   Obtained results from JK-8, it is clear that sediment thickness is about 0.3 km and bore

420   hole touches the Barren-Measures at the depth about 300 m.

421

Number: 1   Author: sanjay   Subject: Replacement Text   Date: 10/25/2016 6:59:00 AM

fault is a well identified boundary where deformation can be seen. here what is meant by metamorphics and sediment?
Author should mark the fault on geological map if it is reported. Figure 2 does not depict any geological fault. it is just a magnetic low surrounded by high.

Number: 2   Author: sanjay   Subject: Replacement Text   Date: 10/25/2016 7:02:18 AM

Rewrite the whole paragraph. it is too difficult to understand many buncombe terminology.

Number: 3   Author: sanjay   Subject: Inserted Text   Date: 10/25/2016 6:59:56 AM

Number: 4   Author: sanjay   Subject: Sticky Note   Date: 10/25/2016 7:05:45 AM

it is worthless to mention about gravity interpretation.
is the author has analysis the gravity data or took some information from published paper.
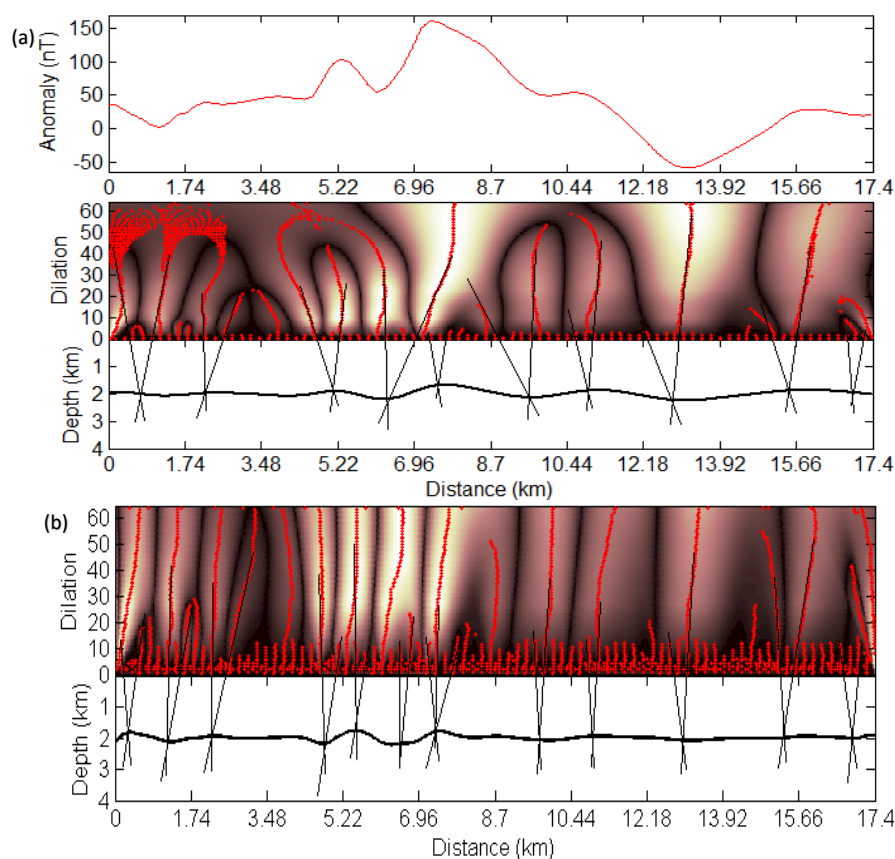
422

423

424   Figure 6 (i): (a) Magnetic anomaly across the profile BB′ and depth estimation by

425   Continuous Wavelet Transform, (b) Depth estimation by Daubechies
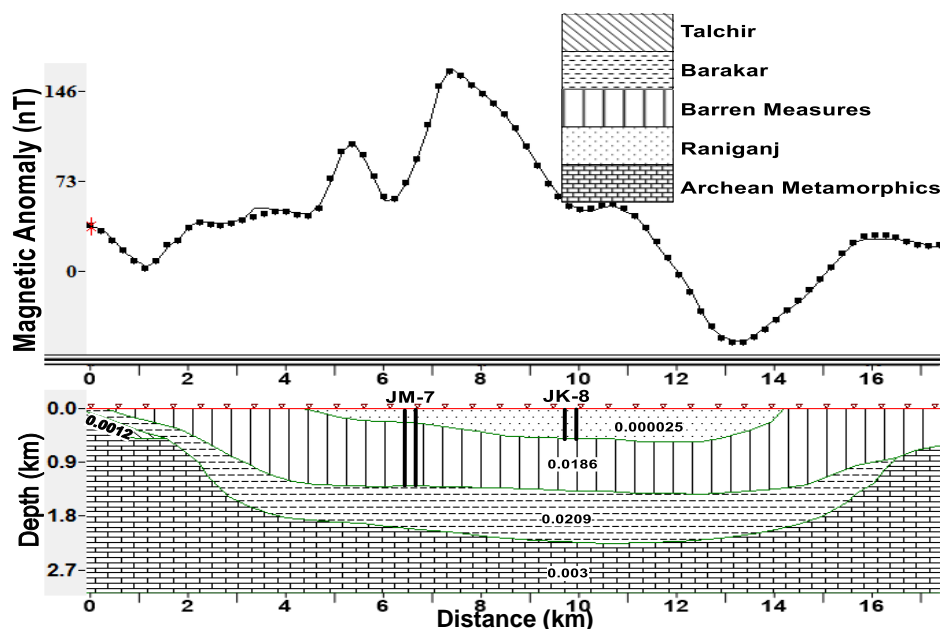
426   wavelet.

Figure 6 (ii): 2D-model of the Profile BB′ drawn in Fig. 2.

The mean depths of causative sources along the profile CC′ (passes west of Mahuda and Katras through Kumardih region, shown in Fig. 2) calculated from the CWT [Fig. 7 (i) (b)] and Daubechies wavelet method [Fig. 7 (i) (b)] varies from 1 km to 2 km. Northern part of the basin shows the flatness in the basin. Most of the sedimentary formations exist along the profile CC′. [Fig. 7 (ii)] reveals that there is a strong indication of both boundaries have slope towards the central part of the basin and the southern boundary is categorized by an abrupt slope than the northern.

Magnetic Field Inclination, Declination and Azimuth Angle of this profile are 36.41º, -0.12º and 268.516º respectively. Gee (1932) mentioned four dykes in the memoir of this coalfield, namely Salama dyke, Sitarampur dyke, Charanpur dyke and Barakar river dyke. The flow of the Barakar river has been shown in Fig. 1. It is remarkable that in this region of this magnetic anomaly profile numbers of ultrabasic dyke (mica peridotites) and sills are found as intrusive into sediments and Barakar formation causes magnetization of the body in the presents earth's field.

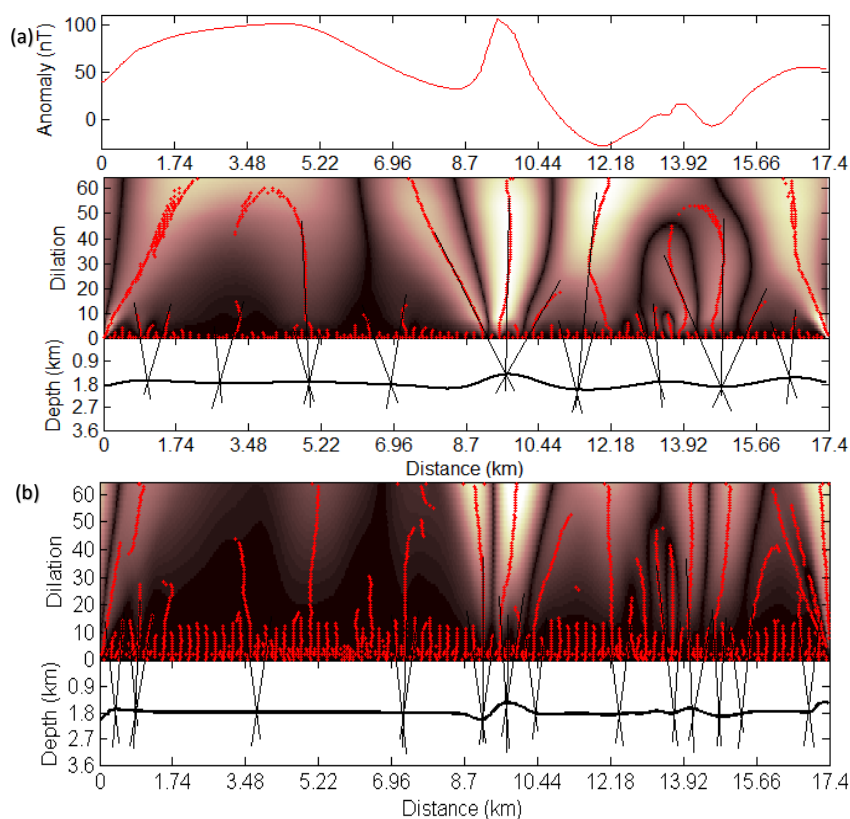Number: 1   Author: sanjay   Subject: Replacement Text   Date: 10/25/2016 7:08:00 AM
The Northern

Geoscientific
Instrumentation
Methods and
Data Systems
Discussions
Open Access

446   Similar to the Profile BB′ Barren measures lies between the Raniganj and Barakar

447   formation. Also, Talchir formation lies between the Barakar and Archean metamorphics

448   whose thickness varies about 1.8 km to 2.2 km at north central part of the basin. The

449   thickness of sediments near Kumardih and Mahuda is about 2.4 km. Moreover, geological

450   sections along the profile CC′ is also based on the results obtained from gravity data, bore

451   hole information as well as geological information. Bore hole NCJA-4, NCJA-5 and MN-

452   11 are located near this profile. Bore hole NCJA-4 and NCJA-5 are located south west of

453   Katras and north east of Kumardih. Depth analysis of individual formation near deepest

454   part of the basin are about 0.4 km for Raniganj formation, 0.95 km for Barren-Measures,

455   0.8 km for Barakar formation and about 0.2 km for Talchir formation.

456

457

458

459

460

Number: 1   Author: sanjay   Subject: Sticky Note   Date: 10/25/2016 7:10:03 AM
mention the reference

461
462
463   Figure 7 (i): (a) Magnetic anomaly across the profile CC′ (drawn in Fig. 2) and depth
464   estimation by Continuous wavelet transform, (b) Depth estimation by
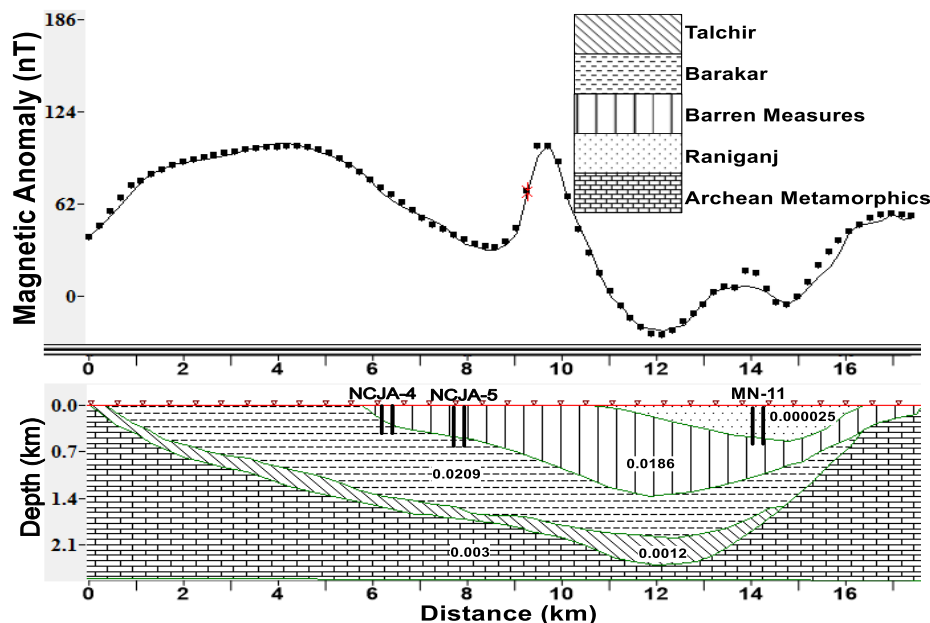465   Daubechies wavelet.
466

Geoscientific
Instrumentation
Methods and
Data Systems
Discussions
Open Access

467
468   Figure 7 (ii): 2D model of the Profile CC′ drawn in Fig. 2.

469

470   The mean depths of causative sources along the profile DD′ (passes east of

471   Mahuda and Katras and west of Parbatpur and Dubrajpur though Barki region, shown in

472   Fig. 2) calculated from the CWT [Fig. 8 (i) (a)] and Daubechies wavelet method [Fig. 8

473   (i) (b)] varies from 1 km to 2.4 km. Also, along this profile there are some indication of

474   fractious contact between the Barakar formation and Barren Measures. Barakar formation

475   appear to pinch out close to the southern boundary fault.

476   Magnetic Field Inclination, Declination and Azimuth Angle of this profile are

477   36.40º, -0.12º and 268.529º respectively. Fault between Barakar formation and

478   metamorpics are clearly indicated by steep gradients of magnetic anomaly at northern end

479   of profile. Southern end of the profile characterized by magnetic variation appears due to

480   an uneven topography. Middle of the profile characterized by a magnetic high of about

481   151 nT because of two dimensional linear feature and magnetic pole which lies nearly

482   0.5-0.65 km below the surface in this region. The extent of Talchir formation assumed to

483   be underlying the Barakar formation is uncertain. Some coal seams exhibit on the surface

484   and northern side have the steep dip than the southern side. Approximate depth of the

485   basement in this area estimated due to single pole at depth of about 2.0 km [Fig. 8 (ii)]

486   below the surface near south west of Parbatpur.

487   Geological sections along this profile also deduced from the analysis of bore hole

488   information, gravity data and geological information. Bore hole NCJA-14, JK-5 and

489   NCJP-32 are located south of Phalmahul, north west of Dubrajpur and west of Parbatpur

490   respectively. The individual maximum thickness of various formations near deepest part

491   of the of the basin are about 0.8 km for Talchir, 0.4 km for Barren-Measure and about 2

492   km for Barakar formation.
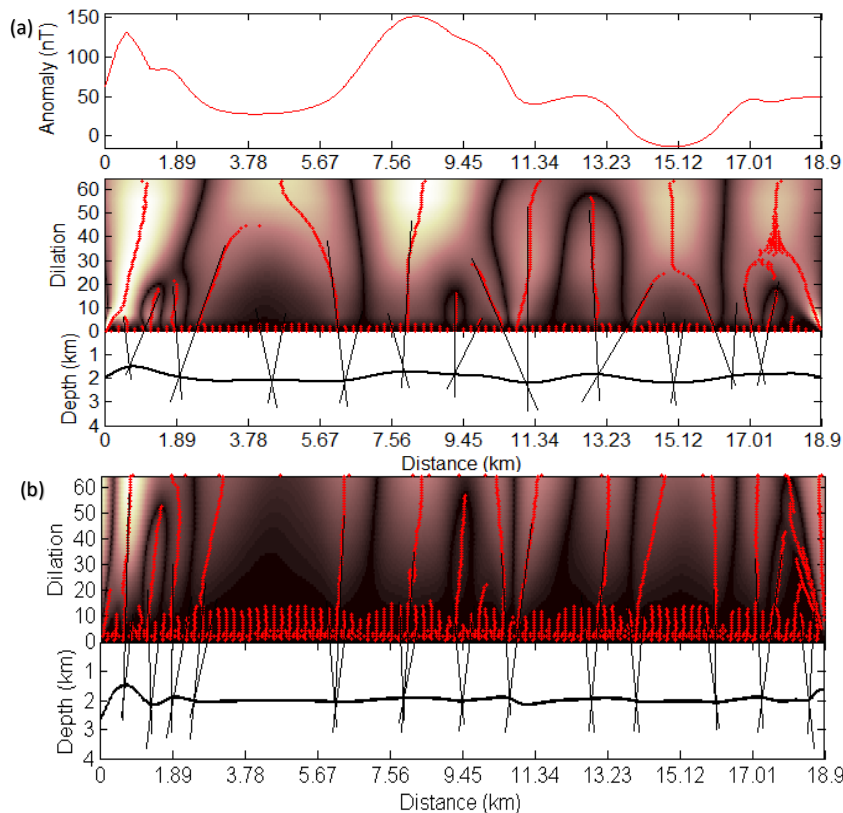
493

494

495

496

497   Figure 8 (i): (a) Magnetic anomaly across the profile DD′ (drawn in Fig. 2) and depth

498   estimation by Continuous Wavelet Transform. (b) Depth estimation by

499   Daubechies wavelet.

Geoscientific
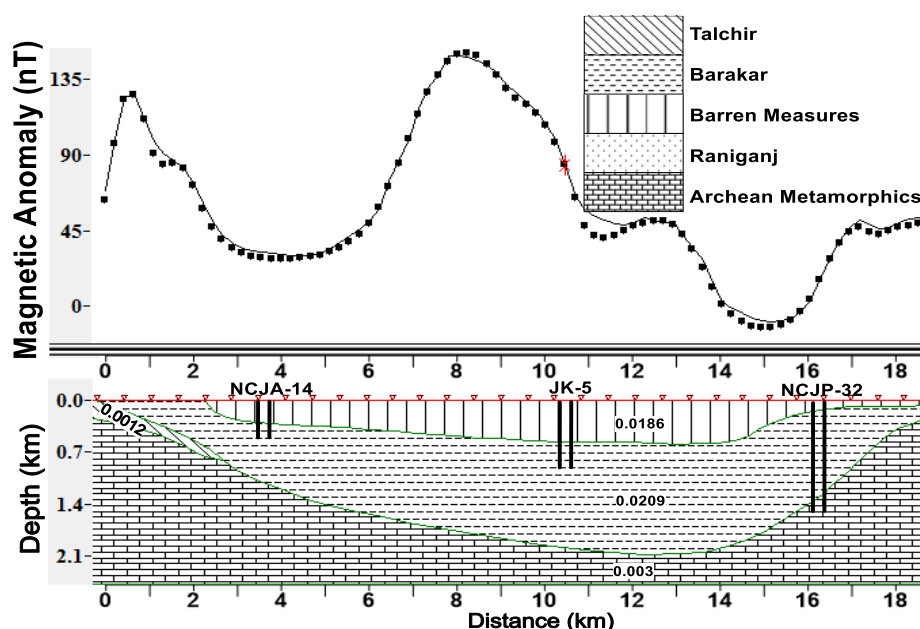Instrumentation
Methods and
Data Systems

Open Access

Discussions

501   Figure 8 (ii): 2D model of the Profile DD′ drawn in Fig. 2.

502

503   The mean depths of causative sources along the profile EE′ (passes east of the

504   Parbatpur and Dubrajpur and west of Dungri, Kustore region, shown in Fig. 2) calculated

505   from the CWT [Fig. 9 (i) (a)] and Daubechies wavelet [Fig. 9 (i) (b)] varies from 1.8 km

506   to 2.8 km. There is a gentle slope of the basin on the northern side, uplift of the basement

507   in the southern part and steep slope close to the southern boundary fault is clearly

508   indicated in this profile.

509   Magnetic Field Inclination, Declination and Azimuth Angle (clockwise from True

510   North) of this profile are 36.39º, -0.12º and 268.556º respectively. Anomaly over this

511   profile can be adequately explained because underlying body having susceptibility

512   contrast with respect to its surrounding. The depth of the basement near the top pole is

513   estimated about 1.5-1.6 km from the surface. Anomaly hike the middle of the profile

514   could be ascribed to the presence of basic or ultrabasic body which was a source for sills

515   and basic dykes which intruded into basin during Precambrian age. The south pole of the

516   underlying source is found to be at a depth of about 0.4 km and the north-pole at 0.7 km

517   depth below the surface [Fig. 9 (ii)]. Eastern margin shows the impact of the occurrence

Number: 1   Author: sanjay   Subject: Highlight   Date: 10/25/2016 11:31:08 AM

Number: 2   Author: sanjay   Subject: Sticky Note   Date: 10/25/2016 7:19:27 AM
is the adequately explained only in DD profile. as we can observe that a high suceptibility contrast exist in all profile.

Number: 3   Author: sanjay   Subject: Highlight   Date: 10/25/2016 7:15:54 AM

Number: 4   Author: sanjay   Subject: Replacement Text   Date: 10/25/2016 7:20:49 AM
in place of hike author should use some appropriate terminology.

Number: 5   Author: sanjay   Subject: Replacement Text   Date: 10/25/2016 7:22:13 AM
what does mean by south pole and north pole.
use appropriate word.

518   of some faults and extension of metamorphic runs under the sediments up to distance of

519   about 1.12 km.

520

521   Geological section along this profile are also deduced from the gravity data, bore

522   hole information and available geological informations. Individual thickness of each

523   formation is also deduced with the help of bore holes JK-4, NCJP-42, NCJP-16 and

524   NCJP-12 which are located south west of Kustor, west of Nunikdih, west of Dungri and

525   south of Dungri respectively. Maximum thickness is about 0.45 km for Barren-Measures,

526   about 1.5 km for Talchir and 1.4 km for Barakar formation have been inferred.
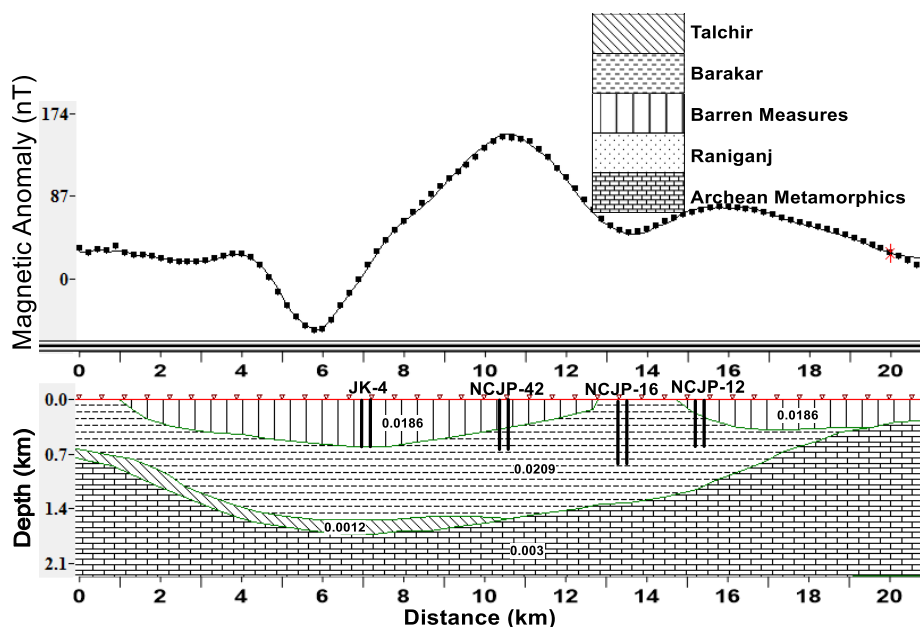
527

528
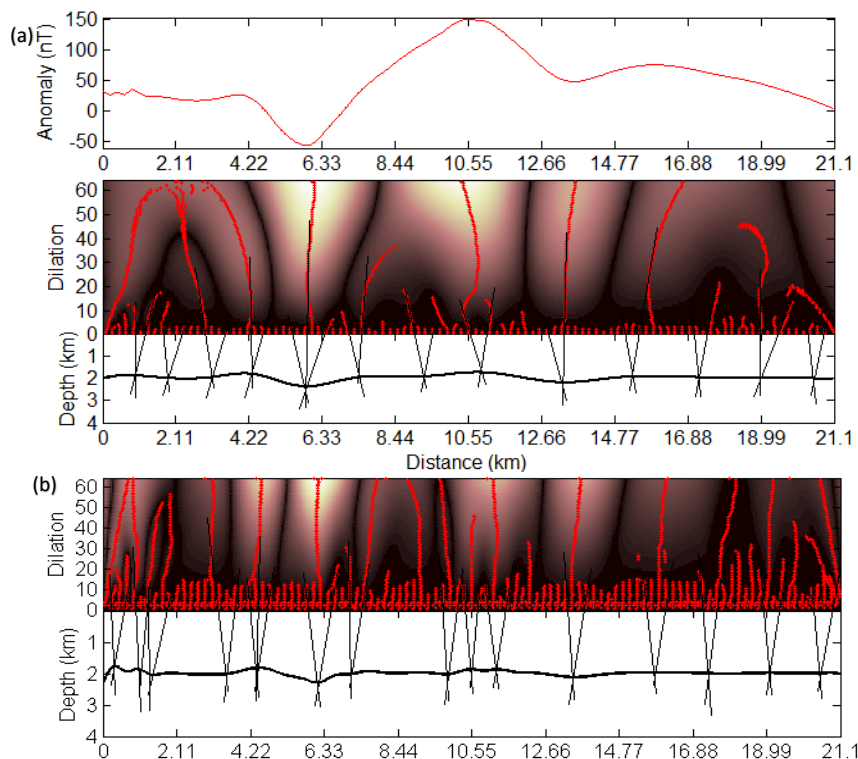
529

530

531   Figure 9 (i): (a) Magnetic anomaly across the profile EE′ (drawn in Fig. 2) and depth

532   estimation by Continuous Wavelet Transform. (b) Depth estimation by

533   Daubechies wavelet.

534

Figure 9 (ii): 2D model of the Profile EE′ drawn in Fig. 2

536

537   The mean depths of causative sources along the profile FF′ (passes east of the

538 Jharia, Dhanbad and west of the Makunda and Pathardih region, shown in Fig. 2)

539 calculated from the CWT [Fig. 10 (i) (a)] and Daubechies wavelet method [Fig. 10 (i)

540 (b)] varies from 1 km to 2.5 km. Also, magnetic anomaly suggest that this area is

541 geologically highly disturbed and dips of the formations varies rapidly.

542   Magnetic Field Inclination, Declination and Azimuth angle of this profile are

543 36.33º, -0.13º and 268.584º respectively. Patherdih horst which is tongue of gneisses

544 penetrates the south east corner of this region. There are strong faults occurs at both ends

545 of the profile. Several interesting possibilities arise regarding the basic intrusives of dykes

546 as well as schists which are normally magnetized. The hike in the anomaly of about 110

547 nT at middle of the profile is due to Peridotite dykes and sills having the close association

548 with Barren-Measure and Barakar formation.

549

550   It is found that in this region of magnetic anomaly remanent magnetization of the

551 body also appears to contribute to the magnetic anomaly. A number of sills and ultrabasic

552 dykes (mica peridotites) are found to be intrusive into the sediments. Geology over this

Number: 1   Author: sanjay   Subject: Replacement Text   Date: 10/25/2016 7:52:36 AM
exaplain the geologically hazardous.

553   profile could be described to the presence of a basic or ultrabasic body which was main

554   source for the sills and basic dykes intruded [Fig. 10 (ii)] into the basin during Gondwana

555   times (Verma et al., 1973).

556

557   Geological strata along this profile are highly disturbed. Therefore, dip of the

558   formations varies abruptly. The thickness of the formations is extrapolated from gravity

559   data, bore holes NCJB-9, NCJB-25 and JFT-8 information as well as geological

560   information. Bore hole NCJB-9, NCJB-25 and JFT-8 are located west of Chhatabad, west

561   of Patherdih and west of Bhojudih respectively. Borehole JFT-8 has the cross contact

562   between Barren-Measures and Barakar formation and it touches the metamorphics at

563   about 0.4 km near west of Bhojudih. The depth of the individual formations are

564   approximately equal to the depth obtained from interpretation of gravity data (Singh and

565   Singh, 2015).

566

567
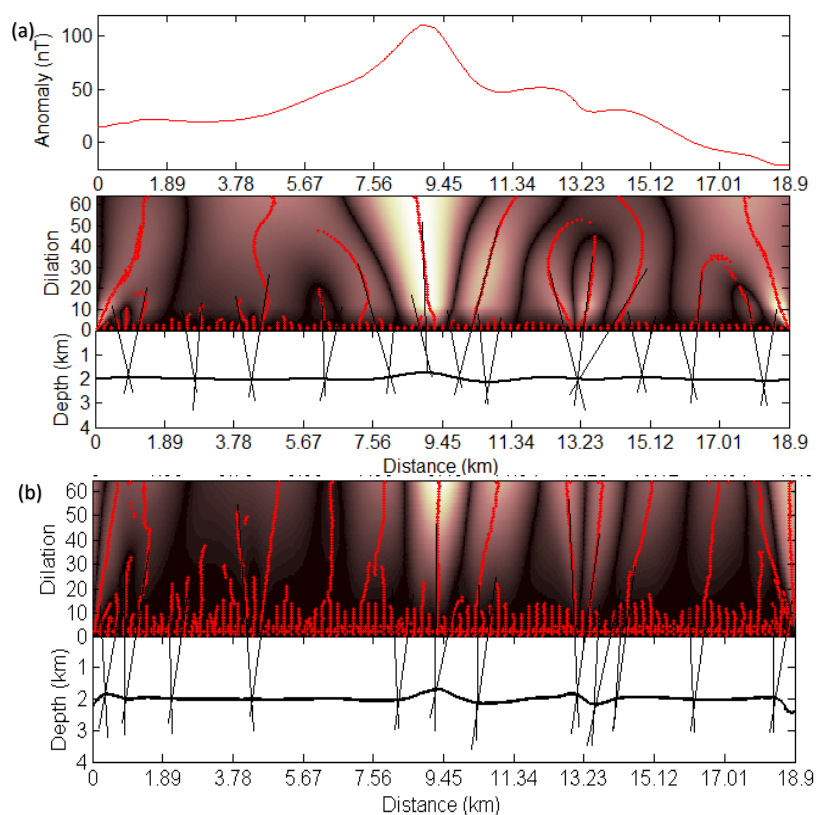
568

569   Figure 10 (i): (a) Magnetic anomaly across the profile FF′ (drawn in Fig. 2) and depth

570   estimation by Continuous Wavelet Transform. (b) Depth estimation by

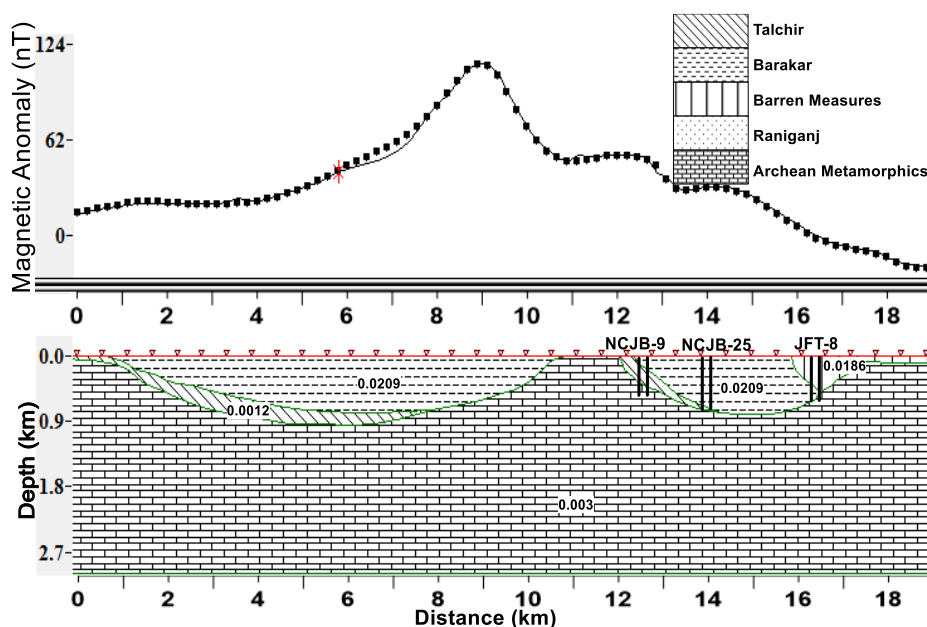571   Daubechies wavelet.

572

573

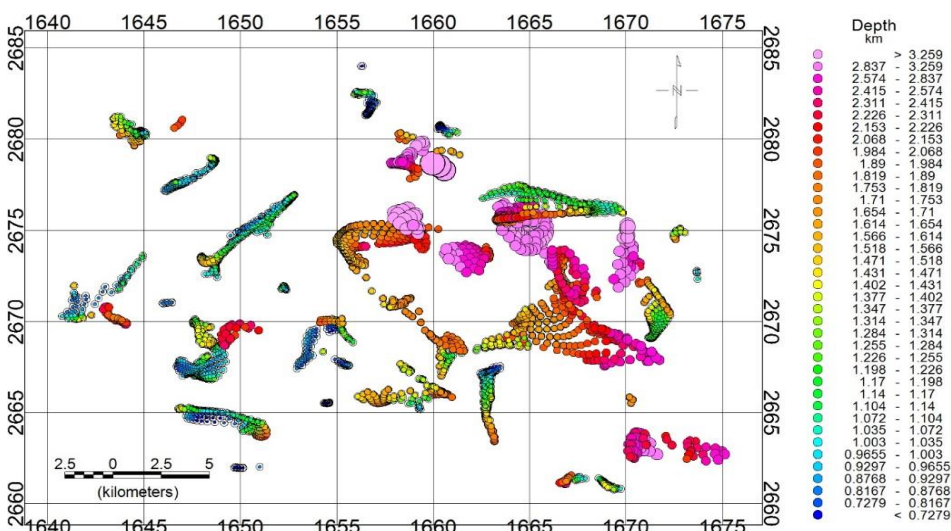574   Figure 10 (ii): 2D model of the Profile FF′ drawn in Fig. 2

575

576

577

578

579   Figure 11: The depth estimates obtained from Euler deconvolution (SI=2) are plotted

580   over UTM coordinates of the study region.

Number: 1   Author: sanjay   Subject: Replacement Text   Date: 10/25/2016 9:51:19 AM
in

Geoscientific
Instrumentation
Methods and
Data Systems
Discussions

Open Access

EGU

581   The interpretation of magnetic anomaly over Jharia coalfield compared with some

582   information from interpretation of gravity data (Verma and Ghosh, 1974). The mean

583   depth to the causative sources of magnetic anomaly estimated by Euler deconvolution

584   method (Fig. 11) ranges about 0.6 km to 3.2 km. The mean depth of the profiles has been

585   shown in the table 1.

586   ~~Algorithm of Euler deconvolution to the total magnetic field anomaly from the~~

587   ~~Jharia coalfield (Fig. 2).~~ magnetic field anomaly is predominantly due to irregular

588   ~~fluctuation~~ of Precambrian outcrops and faults. The magnetic data are sampled at roughly

589   50 m along the profile direction. To enhance the signal to noise ratio, a high cut filter was

590   applied in the wavenumber domain and partial derivative in the vertical direction was

591   obtained by extending the field grid before the calculation. The SI is supposed to vary

592   between 0 and 3 covering all plausible geological bodies. The estimates of source location

593   and depth are obtained by minimizing the error function using nonlinear optimization

594   technique of Coleman and Li (1996).

595   Fig. 11 shows two sets of fractures, predominantly oriented in the NE and SE at

596   northern and southern boundary respectively. The orientation of fracture set agrees with

597   the orientation obtained from regional magnetic interpretation (Verma et al. 1973). In the

598   southern region, the depth of the Precambrian basement derived from the faults less

599   than that in the northern region. Furthermore, intense fracturing is detected in the centre

600   of the study area. In the western and southern region, the source depth is shallow

601   compared to that of the eastern and northern region.

602

603   It suggesting that the most of sediments lies below 700 m, which is reasonable as

604   calculated by wavelet transform method. The intense fracturing at the both north and

605   south boundary grid produces sharp basement between them as observed in the

606   bathymetry. Thus, the faults and depths obtained from the Euler deconvolution, CWT and

607   Daubechies wavelet are related to each other as results obtained from the regional

608   magnetic interpretation.

609

610

611

612

Number: 1   Author: sanjay   Subject: Sticky Note   Date: 10/25/2016 9:56:30 AM
is magnetic anomaly reflect the outcrops feature not the sediment or basement undulation effects?
remove the paragarph as it does not bring out any meaningful or rewrite.

Number: 2   Author: sanjay   Subject: Replacement Text   Date: 10/25/2016 9:52:45 AM
what does mean by algothrim in fig 2. in complete sentence

Number: 3   Author: sanjay   Subject: Replacement Text   Date: 10/25/2016 9:54:04 AM
undulation.

Number: 4   Author: sanjay   Subject: Sticky Note   Date: 10/25/2016 9:57:22 AM
marks the circle in figure 11.

Number: 5   Author: sanjay   Subject: Inserted Text   Date: 10/25/2016 9:58:54 AM
is basement is derived from the fault.

Number: 6   Author: sanjay   Subject: Highlight   Date: 10/25/2016 9:59:34 AM

Number: 7   Author: sanjay   Subject: Highlight   Date: 10/25/2016 10:00:15 AM

Number: 8   Author: sanjay   Subject: Highlight   Date: 10/25/2016 10:01:21 AM

Number: 9   Author: sanjay   Subject: Highlight   Date: 10/25/2016 10:00:08 AM

613 Table 1: Mean depth of 1ources calculated from magnetic anomaly by CWT and
614   Daubechies wavelet along the profiles drawn over Jharia coal field and
615   surrounding regions.
616

Name of Profiles	Distance with depth (km)						
	3	6	9	12	15	18	21
AA′	0.3	0.4	0.38	0.37	0.39	-	-
BB′	2	2.4	2.2	2.5	1.8	-	-
CC′	1.6	1.7	1.2	1.9	2	-	-
DD′	2.2	2.8	1.7	1.8	2.3	-	-
EE′	1.8	2.8	1.8	2	1.7	1.9	2.1
FF′	2.1	2.2	1	1.7	1.8	-	-

617
618

619 Table 2: The following Magnetic susceptibility used to prepare the geological sections.
620 Susceptibility values are taken from the standard chart compiled by Clark and Emerson
621 (1991) and Hunt et al. (1995).

622

Formation	Litho-type	Susceptibility (SI unit)
Raniganj	Fine grained feldspathic sandstones, shales with coal seams	Sandstone=0.0209 Shale=0.0186 Coal=0.000025
Barren Measures	Buff- coloured sandstones, shales and carbonaceous shales	Sandstone=0.0209 Shale=0.0186
Barakar	Buff-coloured coarse and medium-grained feldspathic sandstones, carbonaceous shales, fire clays and coal seams	Sandstone=0.0209 Shale=0.0186 Clay=0.00025 Coal=0.000025
Talchir	Silt, Carbonates Greenish shale and fine grained sandstones	Silt/Carbonates=0.0012 Shale=0.0186 Sandstone=0.0209
Metamorphics	Granite Gneisses, quartzites, mica schists and amphibolites	Granite=0.05 Gneisses=0.025 Quartzites=0.0044 Mica schists=0.003 Amphibolites=0.00075

623
624
625
626

32

| | Number: 1 | Author: sanjay | Subject: Highlight | Date: 10/25/2016 10:04:06 AM |

source of what?
what is number along AA'
pl check the unit of depth. is it in km.

627   **8. Conclusions**

628   It has been shown that CWT allows estimation of the position of the buried source

629   anomalies. For large dilations, the modulus maxima of the CWT and Daubechies wavelet

630   of the magnetic anomalies contain the main features of the location and depth information

631   of anomalous body in the magnetic anomaly. The study over Jharia coal field proves the

632   CWT and Daubechies wavelet method are very efficient to explain the positions of

633   causative sources of potential field (magnetic) data. Extrema lines of these wavelet

634   transforms give satisfactory and reliable informations required to enhance the key

635   parameters of the sources depth and locations.

636

637   The application of the CWT to the synthetic and field magnetic data over Jharia coal

638   fields and surrounding regions demonstrates that the CWT and Euler deconvolution [Fig.

639   16] methods are rapid, easy to execute. Mean depth of causative sources of potential field

640   data obtained from CWT can help to improve qualitative and quantitative interpretation.

641   Also, CWT and Euler deconvolution provide shape of causative sources without any prior

642   knowledge. These methods can play an important role in constructing initial models

643   required for 2-D and 3-D or joint inversion of gravity and magnetic anomalies with better

644   accuracies in very short period.

645

646

647

648

649

650

651

652

653

654

655

656

657

658

Number: 1   Author: sanjay   Subject: Highlight   Date: 10/25/2016 10:04:58 AM

9. References

659

660 Ardestani, E. V., 2010, Precise Edge detection of gravity anomalies by Tilt angle filters,
661   Journal of the Earth & Space Physics, 36, 2, 11-19.

662 Barbosa, V. C. F., Silva, J. B. C. and Medeiros, W. E., 1999, Stability analysis and
663   improvement of structural index estimation in Euler deconvolution, Geophysics, 64,
664   48-60.

665 Blakely, R.J., and Simpson, R.W., 1986, Approximating edges of source bodies from
666   magnetic or gravity anomalies, Geophysics, 51 (7), 1494-1498.

667 Bhattacharyya, B. P., 1972, Tectono-metamorphic effect of granite and pegmatite
668   emplacement in the Precambrian of Bihar Mica Belt. Proc. Symp. On Metallogeny
669   of the Precambrian. Geological Society of India, Bangalore 45-56.

670 Bott, M. H. P. and Ingles, A., 1972, Matrix methods for joint interpretation of two-
671   dimensional gravity and magnetic anomalies with application to the Iceland- Faeroe
672   Ridge, Geophys. J. Roy. Astr. Soc., 30, 55-67.

673 Chamoli, A., Srivastava, R. P. and Dimri, V. P., 2006, Source depth characterization of
674   potential field data of Bay of Bengal by continuous wavelet transform, Indian
675   Journal of Marine Sciences, 35(3), 195-204.

676 Clark, D.A., and Emerson, D.W., 1991, Notes on rock magnetization characteristics in
677   applied geophysical studies, Exploration Geophysics, 22, 547-55.

678 Cooper, G. R. J., 2004, A semi-automatic procedure for the interpretation of geophysical
679   data, Exploration Geophysics, 35, 180-185.

680 Cooper, G. R. I. and Cowan, D. R., 2006, Enhancing potential field data using filters
681   based on the local phase, Comp. & Geoscience, 32, 1585-1591.

682 Cooper, G. R. J. and Cowan Duncan R., 2008, Edge enhancement of potential field data
683   using normalized statistics, Geophysics, 73(3), H1-H4.

684 Cooper, G. R. J., 2011, The semiautomatic interpretation of gravity profile data. Comp.
685   & Geoscience, 37, 1102-1109.

Geoscientific
Instrumentation
Methods and
Data Systems

Open Access

Discussions

EGU

686   Coleman, T. F. and Y. Li., 1996, An interior, trust region approach for nonlinear
687   minimization subject to bounds, SIAM J. on Optimization, 6, 418-445.

688   Dewangan, P., Ramprasad, T., Ramana, M. V., Desa, M. and Shailaja, B., 2007,
689   Automatic interpretation of magnetic data using Euler deconvolution with nonlinear
690   background, Pure and Applied Geophysics, 164, 2359-2372.

691   Fernández Martínez, J. L., Fernández Muñiz, Z., Pallero, J. L. G., Pedruelo González, L.
692   M., 2013, From Bayes to Tarantola: New insights to understand uncertainty in
693   inverse problems, Journal of Applied Geophysics, 98, 62-72.

694   Fernández Martínez, J. L., Fernández Muñiz, M. Zulima., Tompkins, Michael J., 2012,
695   On the topography of the cost functional in linear and nonlinear inverse problems,
696   Geophysics, 77, W1-W15.

697   FitzGerald, D., Reid A., and McInerney, P., 2004, New discrimination techniques for
698   Euler deconvolution, Comp. & Geoscience, 30, 461-469.

699   Fox, C. S., 1930.The Jharia Coal Field, Geological Survey of India, Memoir, 56, 253.

700   Gallardo Delgado, L. A., Perez Flores, M. A. and Gomez Trevino, E., 2003, A versatile
701   algorithm for joint 3D inversion of gravity and magnetic data, Geophysics, 68, 949-
702   959.

703   Gerovska, D. and Arauzo Bravo, M. J., 2003, Automatic interpretation of magnetic data
704   based on Euler deconvolution with unprescribed structural index, Comp. &
705   Geoscience, 29, 949-960.

706   Gee, E. R., 1932, The geology and coal resources of the Raniganj coalfield, Mem. Geol.
707   Surv. India, 61, 1-343.

708   Goyal, P. and Tiwari, V. M., 2014, Application of the continuous wavelet transform of
709   gravity and magnetic data to estimate sub-basalt sediment thickness, Geophysical
710   Prospecting, 62, 148-157.

711   Gunn, P. J., 1975, Linear transformations of gravity and magnetic fields, Geophysical
712   Prospecting, 23, 300-312.

Geoscientific
Instrumentation
Methods and
Data Systems
Discussions

713   Hunt, C. P., Moskowitz, B.M. and Banerjee, S.K., 1995, Magnetic properties of Rocks
714   and Minerals, In: Rock Physics and Phase Relations - A hand book of Physical
715   constants, AGU Reference shelf 3, etd. Ahrens, T. J., 189-204.

716   Hsu, S. K., Sibuet, J. C. and Shyu, C. T., 1996, High resolution detection of geologic
717   boundaries from potential-field anomalies: an enhanced analytic signal: technique,
718   Geophysics, 61, 373-386.

719   Hsu, S. K., 2002, Imaging magnetic sources using Euler's equation, Geophysical
720   Prospecting, 50, 15-25.

721   Holschneider, M., A. Chambodut, and M. Mandea, 2003, From global to regional analysis
722   of the magnetic field on the sphere using wavelet frames, Physics of the Earth and
723   Planetary Interiors, 135, 107-124.

724   Jiang Fan, Wu Jiansheng and Wang Jialin, 2008, Joint inversion of gravity and magnetic
725   data for a two-layer model, Applied Geophysics, 5, 331-339.

726   Keating, P. B., 1998, Weighted Euler deconvolution of gravity data, Geophysics, 63,
727   1595-1603.

728   Kopal, Z., 1961, Numerical analysis, Chapman and Hall Ltd., London, 551-553.

729   Melo, F. F., Barbosa, V. C. F., Uieda, L., Oliveira Jr, V. C. and Silva, J. B. C., 2013,
730   Estimating the nature and the horizontal and vertical positions of 3D magnetic
731   sources using Euler deconvolution, Geophysics, 78, J87-J98.

732   Menichetti, V., and Guillen, A., 1983, Simultaneous interactive magnetic and gravity
733   inversion, Geophysical Prospecting, 31, 929-994.

734   Moreau, F., Gibert, D., Holschneider, M. and Saracco, G., 1997, Wavelet analysis of
735   potential fields, Inverse Problems, 13, 165-178.

736   Moreau, F., Gibert, D., Holschneider, M., and Saracco, G., 1999, Identification of sources
737   of potential fields with continuous wavelet transform: Basic theory, Journal of
738   Geophysical Research, 104, 5003-5013.

Geoscientific
Instrumentation
Methods and
Data Systems
Discussions

Open Access

EGU

739 Mushayandebvu, M. F., Van, Driel P., Reid, A. B., and Fairhead, J. D., 2001, Magnetic
740   source parameters of two dimensional structures using extended Euler
741   deconvolution, Geophysics, 66, 814-823.

742 Mushayandebvu, M. F., Lesur, V., Reid, A. B., and Fairhead, J. D., 2004, Grid Euler
743   deconvolution with constraints for 2D structures, Geophysics, 69, 489-496.

744 Perez, Wijns, C. C. and Kowalczyk, P., 2005, Theta map: Edge detection in magnetic
745   data: Geophysics, 70(4), L39-L43.

746 Pilkington, M., 2006, Joint inversion of gravity and magnetic data for two layer models,
747   Geophysics, 71, 35-42.

748 Raja Rao, C. S., 1987, Coalfield of India, v.IV (pt.1) Bull. Geol. Surv. India, Series A,
749   45, 336.

750 Ravat, D., 1996, Analysis of the Euler method and its applicability in environmental
751   investigations, Journal of Environmental and Engineering Geophysics, 1, 229-238.

752 Reid, A. B., Allsop, J. M., Granser, H., Millet, A. J. and Somerton, I. W., 1990, Magnetic
753   interpretation in three dimensions using Euler deconvolution, Geophysics, 55, 80-
754   91.

755 Reid, A. B., Ebbing, J. and Webb, S. J., 2014, Avoidable Euler Errors- the use and abuse
756   of Euler deconvolution applied to potential field, Geophysical Prospecting, 62,
757   1162-1168.

758 Salem, A., Williams, S., Fairhead, J. D., Ravat, D. and R. Smith, 2007, Tilt-depth method:
759   a simple depth estimation method using first order magnetic derivatives, The
760   Leading Edge, 26/12, 1502-1505.

761 Sailhac, P., Gibert, D. and Boukerbout, H., 2009, The theory of the continuous wavelet
762   transform in the interpretation of potential fields: A review, Geophysical
763   Prospecting, 57, 517-525.

764 Silva, J. B. C., Barbosa, V. C. F. and Medeiros, W. E., 2001, Scattering, symmetry, and
765   bias analysis of source position estimates in Euler deconvolution and its practical
766   implications, Geophysics, 66, 1149-1156.

Geoscientific
Instrumentation
Methods and
Data Systems
Discussions
Open Access
EGU

767   Silva, J. B. C. and Barbosa, V. C. F., 2003, 3D Euler deconvolution: Theoretical basis for
768   automatically selecting good solutions, Geophysics, 68, 1962-1968.

769   Singh, A. and Singh, U. K., 2015, Wavelet analysis of residual gravity anomaly profiles:
770   Modeling of Jharia coal basin, India, 86 (6), 679–686.

771   Stavrev, P. and Reid, A., 2007, Degrees of homogeneity of potential fields and structural
772   indices of Euler deconvolution, Geophysics, 72, L1-L12.

773   Stavrev, P. Y., 1997, Euler deconvolution using differential similarity transformations of
774   gravity or magnetic anomalies, Geophysical Prospecting, 45, 207-246.

775   Thompson, D. T., 1982, EULDPH: A new technique for making computer assisted depth
776   estimates from magnetic data, Geophysics, 47 (1), 31-37.

777   Verma, R. K., Bhuin, N. C. and Mukhopadhyay, M., 1979, Geology, Structure and
778   tectonics of Jharia Coal Field, India- A 3-D Model, Geoexploration, 17, 305-324.

779   Verma, R. K. and Ghosh, D., 1974, Gravity survey over Jharia coalfield, India. Geophys.
780   Res. Bull., 12, 165-175.

781   Verma, R. K., Majumdar, R., Ghosh, Debabrata, Ghosh, Ashish and Gupta, N. C., 1976,
782   Results of Gravity Survey over Raniganj Coalfield, India, Geophysical Prospecting,
783   24, 19-30.

784   Verma, R. K., Prasad, S. N. and Jha, B. P., 1973, Magnetic Survey over Jharia Coal Field,
785   Pure and Applied Geophysics, 102 (1), 124-133.

786   Williams, S., Fairhead, J. D. and Flanagan, G., 2003, Grid based Euler deconvolution:
787   Completing the circle with 2D constrained Euler, SEG Technical Program
788   Expanded Abstracts, 22, 576-579.

789   Wu, J. S., Jiang, F. and Wang, J. L., 2007, Study of joint inversion of gravity and magnetic
790   data for variable density interface model, Proceeding of Annual of the Chinese
791   Geophysical Society, 633.

792   Zeyen, H. and J. Pous, 1993, 3-D joint inversion of magnetic and gravimetric data with a
793   priori information, Geophysical Journal International, 112, 244-256.

Geoscientific
Instrumentation
Methods and
Data Systems
Discussions

Open Access

794   Zhang, C., Mushayandebvu, M. F., Reid, A. B., Fairhead, J. D. and Odegard, M. E., 2000,

795   Euler deconvolution of gravity tensor gradient data, Geophysics, 65, 512-520.

796   Zhang, G. B., Shen, N. H., Wang, X. C. and Wang, H. X., 1993, The program system on

797   generalized linear cooperative inversion of the potential anomalies, Journal of

798   Changchun University (Earth Sciences), 23(2), 197-204.